A redundant rehabilitation robot with a variable stiffness mechanism

Carl Nelson, Laurence Nouaille, Gérard Poisson

Mechanism and Machine Theory

A Redundant Rehabilitation Robot with a Variable Stiffness Mechanism

--Manuscript Draft--

Manuscript Number:	MECHMT-D-19-00272
Article Type:	Research Paper
Keywords:	Variable Stiffness; Robotic Rehabilitation; Redundant Robot; Compliant Mechanisms
Corresponding Author:	Carl Nelson University of Nebraska-Lincoln NE UNITED STATES
First Author:	Carl Nelson
Order of Authors:	Carl Nelson
	Laurence Nouaille
	Gérard Poisson
Abstract:	This paper presents a variable stiffness mechanism suitable for use in robotic rehabilitation. By inherently varying both the magnitude and direction of loading in the mechanism using a single input, a large variation in effective stiffness is achieved. Design and analysis of the variable stiffness mechanism are presented, along with an example illustrating performance capabilities.
Suggested Reviewers:	
Opposed Reviewers:	

Cover Letter: Mechanism and Machine Theory

12 November, 2019

Dear Editor,

We are pleased to submit this manuscript, titled “A Redundant Rehabilitation Robot with a Variable Stiffness Mechanism,” in consideration for publication in Mechanism and Machine Theory. This work is based in part on a conference article (“Variable Stiffness Mechanism for Robotic Rehabilitation”) which appeared in the proceedings of the 2019 IFToMM World Congress held this year in Poland, but includes substantially new and additional content. We appreciate the opportunity to have this work considered for publication, and remain at your disposal for any necessary information in support of the review process.

Sincerely,

Carl Nelson, professor of mechanical and materials engineering, University of Nebraska-Lincoln

(on behalf of all authors)

A Redundant Rehabilitation Robot with a Variable Stiffness Mechanism

Carl A. Nelson*[a], Laurence Nouaille[b], and Gérard Poisson[b]

[a] University of Nebraska-Lincoln, Lincoln, NE 68588, USA

[b] PRISME Lab, Université d'Orléans INSA-CVL, Bourges, France

* corresponding author, cnelson5@unl.edu

Abstract:

This paper presents a variable stiffness mechanism suitable for use in robotic rehabilitation. By inherently varying both the magnitude and direction of loading in the mechanism using a single input, a large variation in effective stiffness is achieved. Design and analysis of the variable stiffness mechanism are presented, along with an example illustrating performance capabilities.

This paper presents a serial robot for upper limb rehabilitation whose noteworthy characteristics are a degree of redundancy and variable stiffness in its four active degrees of freedom. These traits make the robot suitable for various rehabilitation tasks. The kinematic solution is derived, and simulations of two characteristic movements demonstrate how the variable stiffness and redundancy contribute to task performance.

Keywords: Variable Stiffness, Robotic Rehabilitation, Redundant Robot, Compliant Mechanisms.

Highlights:

- New variable stiffness device
- Integration of variable stiffness in a robot design
- Analysis of effects of variable stiffness on overall robot performance

1 Introduction

With improvements in health care, populations are aging [1], and it is becoming ever more important to focus on maintaining quality of life into the later years. Additionally, many millions of people worldwide are living with disabilities, whether caused by injury or illness, which cause upper limb weakness and negatively impact the ability to participate in activities of daily living (ADL) [2]. To be effective, therapeutic strategies for augmenting and training weak muscles require mass repetition of meaningful, everyday tasks, as well as progressive variation in the amount of assistance or correction provided. These factors motivate the creation of robotic rehabilitation technology to maximize quality of life.

However, current technologies tend to be either low-tech and affordable (e.g., "slings and springs" that provide the most basic level of assistance) or high-tech and expensive (e.g., robots using feedback control to vary assistance). This latter category is limited by factors such as cost, portability, and general availability of these devices. Simple and low-cost "variable-stiffness" features in robotic therapy devices are needed to promote functional independence. It should be noted that since the most common way to achieve variable stiffness is through high-bandwidth control approaches [3], this limits the ability to reduce cost in these systems.

Existing robotic devices for arm rehabilitation have proliferated in recent years. Examples include ArmeoPower, ARM guide [4], ARMin [5], Bi-Manu-Track [6], GENTLE/s [7], InMotion ARM, MIME [8], MIT-Manus [9], Myomo, T-WREX/Armeo Spring [10-12] among many others. However, a recent review of more than 120 upper extremity rehabilitation robots [13] shows that commercially available solutions are few in number and range from somewhat portable, low-DOF systems (e.g., Myomo, a 1-DOF elbow orthosis) to stationary, high-DOF systems (e.g., ArmeoPower, a 7-DOF exoskeleton). These can generally be classified as either joint-by-joint (exoskeleton) designs (e.g., ArmeoPower) or end effector-type systems in which a particular point on the limb is guided (e.g., InMotion ARM). The review revealed that while there is no shortage in the development of robotic systems for arm rehabilitation, there is a significant technology gap pertaining to the simple, low-cost implementation of variable-stiffness features using those systems.

In light of robots' potential interactions with humans, one of the key technological limitations of most robot designs is their relatively high stiffness, which is compounded by the difficulty of modifying this property on the fly. An ideal robot for robotic rehabilitation would be lightweight, have low inertia, provide adequate power for a range of tasks, and allow a range of impedance or stiffness characteristics, all while being inherently safe. In a recent review of upper extremity rehabilitation robots and their control modes [14], it was pointed out that rehabilitation tasks may be assistive, resistive, or corrective in nature. This spectrum of functionality necessitates variable, anisotropic stiffness as a property of rehabilitation robots, particularly when accounting for inter-patient variability and the evolving needs of each individual patient over time.

In a recent review of variable-stiffness actuators, Vanderborght [3] used a four-category classification: variable stiffness using control, inherent compliance, inherent damping, and inertial variation. Numerous drawbacks to the control-based approach were identified, including difficulty handling shock loading, storing and releasing energy, and exploiting energy-efficient natural dynamics, as well as the general complexity and need for accurate dynamic models. Although varying effective stiffness through control software is probably the most common way that human-robot interaction is implemented, another key drawback in the context of assistive robotics is that

this requires expensive, high-performance actuator systems to provide the needed bandwidth for an appropriate stiffness range characteristic of human interaction tasks.

The main drawback of variable-damping devices (e.g., friction-based, fluidic, electro-rheological, magneto-rheological) is that they are energy-dissipating devices and thus inefficient. Inertial devices use flywheels or gyroscopic effects to modulate inertial forces and thus change the apparent stiffness; these devices can be bulky, store a lot of energy, and may suffer from limited bandwidth in terms of system dynamics.

To increase safety and flexibility of use, as well as decrease cost in high-performance actuators, it is desirable for robot stiffness to be mechanically adjustable (a system-level approach to flexible robotics) rather than implemented as a layer of control software; therefore, we favor the category of inherent-compliance devices as classified in Vanderborght [3]. These devices can take various forms and have the advantage of large bandwidth in terms of adjusting to a wide range of stiffnesses and/or natural frequencies. Basic examples include series arrangements of actuators and springs [15,16], though these tend to require high-performance actuators to induce the desired stiffness characteristic through the spring. Likewise, antagonistic arrangements of springs and actuators have been proposed [17-19]. However, these are similarly inefficient because motors have to carry the spring loads. Zhou et al. [20] recently presented an active variable stiffness module using cables and springs in which adjustment of the preloads modulates stiffness. Another recent approach [21] involved an intermediate torque arm with moveable springs to scale the apparent stiffness. Vanderborght et al. [3] classified this type of device as changing the transmission between the load and the spring. Another option is to change the spring properties to vary its stiffness, such as changing the active number of coils [22] or reorienting a beam to alter the effective moment of inertia [23]. Kani et al. [24] created a distributed array of small actuators with springs to produce an overall variable-stiffness actuator pack. These approaches appear to suffer from various disadvantages, such as increased bulk and mechanical complexity [20-21,24], limited stiffness range [21,23], and/or poor energy efficiency [17,24].

A somewhat limited body of work has focused on using a lever concept to enable variable stiffness in a compact actuator package. In Tsagarakis [25], a cam-type lever arm with an adjustable pivot driven by a rack and gear mechanism allowed variation of rotational stiffness based on offset linear springs. In a modification of this design [26], the linear springs were replaced with torsion springs and the rack/gear pivot adjustment was replaced with a ball screw. A similar but slightly later design by a different group [27,28] used a Cardan gear mechanism to adjust the pivot point. The advantages shared by these designs are large stiffness range, ease of adjustment, and relatively compact structure. However, they are not easily modularized (they have to be built into each actuator) and this causes a cascade effect into decreased dynamic performance and decreased suitability for robots directly interacting with humans.

In this paper, a simple variable-stiffness transmission is presented which draws on some of the principles from prior literature. Stiffness is adjusted mechanically, using a compliant beam as the stiffness element. Adjustment of the mechanism simultaneously changes the load on the spring element, as well as the orientation of the load with respect to the spring (effectively changing the transmission ratio). The result is a wide range of achievable stiffness properties. We also present a redundant robot for upper limb rehabilitation in which these variable-stiffness elements are inserted between drive motors and joint axes, rather than using control-based approaches with high-performance actuators placed directly on the joints. This concept has been referred to as "inherent compliance" [3] or (more generally) "mechanical intelligence". We describe the robot

design, derive its kinematic relationships, and show how joint stiffnesses are mapped to stiffness at the end effector. Two examples of trajectory-following tasks, relevant to arm rehabilitation, involving deterministic translational and rotational wrist patient movements, have been simulated. They show the ability to control the robot compliance using the variable-stiffness mechanism.

2 System Design

The variable stiffness mechanism (see Figure 1) consists of a primary actuator, a driven rotational joint, a belt coupling, a spring-loaded idler (freely rotating pulley mounted on an elastic beam), and a lead screw with secondary actuator. The lead screw is used to adjust the position of the base of the beam with respect to the primary actuator and driven joint. The belt couples the primary actuator to the driven joint under a no-slip condition, but is also acted upon by the idler mounted on the distal extremity of the beam. Actuation of the lead screw results in variation of the stiffness response of the driven joint with respect to the actuator input. In other words, the result is a variable-stiffness spring acting between the position-controlled input and the output axis. It is assumed that other friction and backdriveability considerations related to gearing are negligible relative to the effects of this "spring" since they would occur primarily on the actuator side of the mechanism.

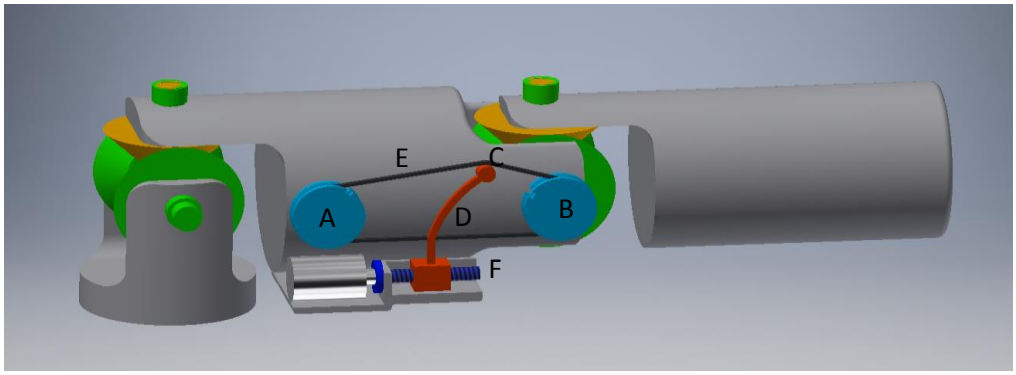

Fig. 1. Representation of the variable stiffness mechanism mounted on a robot arm (driving a differential mechanism); A: driving joint (actuator), B: driven joint, C: freely rotating idler, D: beam spring, E: belt, F: lead screw.

3 Robot Design

The robot consists of two serial links connected by actuated differentials (universal joints), giving the robot a total of four degrees of freedom (DOF). The end effector can be thought of as a passive spherical joint attached to the wrist or forearm of the patient to facilitate path-following tasks. The robot is therefore suitable for 3-DOF arm guidance tasks, possessing 1 degree of redundancy. As seen in Figure 2, since the most distal active joint is in the differential at the base of the second link, it is possible for the second (distal) link to be slim and lightweight, since its drive motors can be mounted on the proximal link.

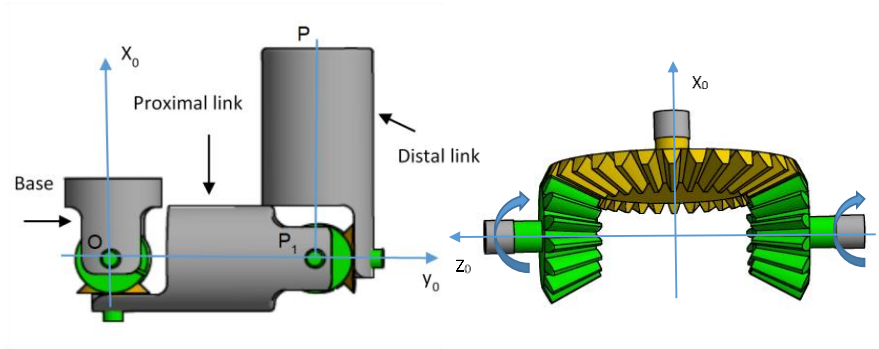

Fig. 2. Representation of redundant double-differential robot and differential joint.

4 Kinematic Analysis

We define L_1 and L_2 as the two dimensional parameters of the robot and θ_1 to θ_4 as the four joint variables. Referring to the body-fixed reference frames of the robot in Figure 3, the incremental transformations are as follows.

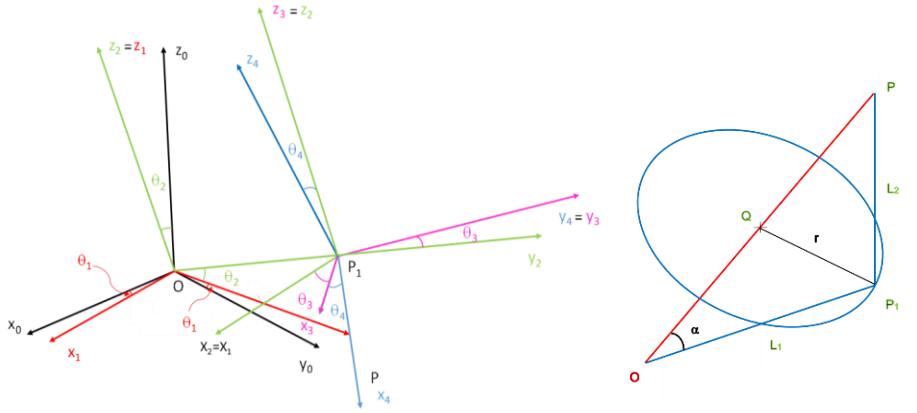

Fig. 3. Kinematic reference frames (left); redundancy of elbow position (right).

$$ {}^0T_1 = R_z(\theta_1),\ {}^1T_2 = R_x(\theta_2),\ {}^2T_3 = S_y(L_1),\ {}^3T_4 = R_z(\theta_3),\ {}^4T_5 = R_y(\theta_4),\ {}^5T_6 = S_x(L_2) \quad (1) $$

The end-effector transformation is (using s and c to represent sin and cos respectively):

$$ T = {}^0T_1\,{}^1T_2\,{}^2T_3\,{}^3T_4\,{}^4T_5\,{}^5T_6 = \quad (2) $$

$$ \begin{bmatrix} c_1c_3c_4 - s_1c_2s_3c_4 - s_1s_2s_4 & -c_1s_3 - s_1c_2c_3 & c_1c_3s_4 - s_1c_2s_3s_4 + s_1s_2c_4 & -L_1s_1c_2 + L_2(c_1c_3c_4 - s_1c_2s_3c_4 - s_1s_2s_4) \\ s_1c_3c_4 + c_1c_2s_3c_4 + c_1s_2s_4 & -s_1s_3 + c_1c_2c_3 & s_1c_3s_4 + c_1c_2s_3s_4 - c_1s_2c_4 & L_1c_1c_2 + L_2(s_1c_3c_4 + c_1c_2s_3c_4 + c_1s_2s_4) \\ s_2s_3c_4 - c_2s_4 & s_2c_3 & s_2s_3s_4 + c_2c_4 & L_1s_2 + L_2(s_2s_3c_4 - c_2s_4) \end{bmatrix} $$

and the end-effector position is

$$ P = [P_x\ P_y\ P_z\ 1]^T = T[0\ 0\ 0\ 1]^T = [t_{14}\ t_{24}\ t_{34}\ 1]^T \quad (3) $$

With one degree of redundancy, the robot has an infinite number of solutions for following a desired set of waypoints along a trajectory. A classical method of resolving the redundancy would be to increment from an initial position using a Jacobian pseudoinverse approach which minimizes joint motion along the trajectory:

$$\Delta\theta = J^T (J J^T)^{-1} \Delta P \quad (4)$$

Here we pursue a more direct and ultimately more flexible approach for resolving the redundancy, which we believe to be novel for this robot. As shown in Figure 2, for any pose P, the redundancy of the 4-DOF robot in reaching a 3-DOF pose in Cartesian space allows the "elbow" of the robot (denoted as P_1) to lie at any point on a circle symmetric about the line OP. This circle can be described by the following system of two equations, one representing a sphere centered at Q and the other constraining the circle to lie in a plane normal to the line OP through Q.

$$(P_{1x} - Q_x)^2 + (P_{1y} - Q_y)^2 + (P_{1z} - Q_z)^2 = r^2 \quad (5)$$

$$Q_x(P_{1x} - Q_x) + Q_y(P_{1y} - Q_y) + Q_z(P_{1z} - Q_z) = 0 \quad (6)$$

Here, r is the radius of the circle (locus of P_1) and is given by

$$r = L_1 \sin\alpha \quad (7)$$

where α is found using the law of cosines in the triangle POP_1:

$$\cos\alpha = (L_1^2 + |OP|^2 - L_2^2)/(2L_1|OP|) \quad (8)$$

$$|OP| = (P_x^2 + P_y^2 + P_z^2)^{1/2} \quad (9)$$

From the trigonometry of this construction, point Q is given by a scalar multiple of P:

$$[Q_x\ Q_y\ Q_z]^T = (L_1\cos\alpha/|OP|)[P_x\ P_y\ P_z]^T = ((L_1^2 + |OP|^2 - L_2^2)/(2|OP|^2))\ [P_x\ P_y\ P_z]^T \quad (10)$$

With point Q determined, the preceding pair of equations which describe the circle (locus of P_1) are readily solved for a unique value of P_1 (elbow location) by the addition of one constraint. For example, specifying any one of $\{P_{1x}, P_{1y}, P_{1z}\}$ and substituting the orthogonality constraint into the equation of the sphere leads to a quadratic equation in the remaining variable. This can be used to assign P_1 a value which avoids obstacles in the workspace (e.g., in the arm rehabilitation setting, obstacles could include the patient's body or objects with which the patient is asked to interact).

With P_1 determined, it is possible to obtain a closed-form solution to the inverse kinematics by dividing the problem into two parts: using P_1 to solve for θ_1 and θ_2, and then using the desired end-effector position P to solve for the remaining θ_3 and θ_4. With

$$T_{P1} = {}^0T_1\ {}^1T_2\ {}^2T_3 \quad (11)$$

the elbow position can be expressed with components

$$[P_{1x}, P_{1y}, P_{1z}]^T = [-L_1 s_1 c_2, L_1 c_1 c_2, L_1 s_2]^T \quad (12)$$

Solving these equations for the joint variables gives

$$\theta_1 = \tan^{-1}(-P_{1x}/P_{1y}) \quad (13)$$

$$\theta_2 = \sin^{-1}(P_{1z}/L_1) \quad (14)$$

With these two joint variables determined, the remaining two joint variables can be found by standard algebraic elimination and trigonometric identities applied to the expression for point P:

$$\theta_3 = \tan^{-1}\left(\frac{(P_z - P_{1z})s_2 + (P_y - P_{1y})c_1 c_2 - (P_x - P_{1x})s_1 c_2}{(P_x - P_{1x})c_1 + (P_y - P_{1y})s_1}\right) \quad (15)$$

$$\theta_4 = \sin^{-1}\left(\frac{-(P_z - P_{1z})c_2 + (P_y - P_{1y})c_1 s_2 - (P_x - P_{1x})s_1 s_2}{L_2}\right) \qquad (16)$$

Finally, since these four joint variables are actually driven through differentials (as illustrated in Figure 1), the true input variables can be denoted ϕ_i (i = 1…4) with the following forward and inverse transformations:

$$\theta_1 = \tfrac{1}{2}(\phi_1 - \phi_2), \quad \theta_2 = \tfrac{1}{2}(\phi_1 + \phi_2), \quad \theta_3 = \tfrac{1}{2}(\phi_3 - \phi_4), \quad \theta_4 = \tfrac{1}{2}(\phi_3 + \phi_4)$$

$$\phi_1 = \theta_1 + \theta_2, \quad \phi_2 = \theta_2 - \theta_1, \quad \phi_3 = \theta_3 + \theta_4, \quad \phi_4 = \theta_4 - \theta_3 \qquad (17)$$

Differentiating the expression for P above gives the 3×4 position Jacobian ${}^{\theta}J$ in terms of $\theta_{1\text{-}4}$.

$${}^{\theta}J =$$

$$\begin{bmatrix} -L_1c_1c_2 - L_2(s_1c_3c_4 + c_1c_2s_3c_4 + c_1s_2s_4) & L_1s_1s_2 + L_2(s_1s_2s_3c_4 - s_1c_2s_4) & -L_2(c_1s_3c_4 + s_1c_2c_3c_4) & L_2(-c_1c_3s_4 + s_1c_2s_3s_4 - s_1s_2c_4) \\ -L_1s_1c_2 + L_2(c_1c_3c_4 - s_1c_2s_3c_4 - s_1s_2s_4) & -L_1c_1s_2 + L_2(-c_1s_2s_3c_4 + c_1c_2s_4) & L_2(-s_1s_3c_4 + c_1c_2c_3c_4) & L_2(-s_1c_3s_4 - c_1c_2s_3s_4 + c_1s_2c_4) \\ 0 & L_1c_2 + L_2(c_2s_3c_4 + s_2s_4) & L_2(s_2c_3c_4) & -L_2(s_2s_3s_4 + c_2c_4) \end{bmatrix} \qquad (18)$$

With respect to the actual input angles ϕ, based on their relationships with θ, the Jacobian is:

$$J = \frac{1}{2}\,{}^{\theta}J \begin{bmatrix} 1 & -1 & 0 & 0 \\ 1 & 1 & 0 & 0 \\ 0 & 0 & 1 & -1 \\ 0 & 0 & 1 & 1 \end{bmatrix} \qquad (19)$$

5 Stiffness analysis

The Jacobian can be used to map the stiffness relationships between the local joint space and the global frame of reference as follows. The Jacobian is defined by

$$\delta P = J\delta\theta \qquad (20)$$

and also relates loading in the local and global reference frames:

$$\tau = J^T F \qquad (21)$$

where τ is the vector of generalized joint efforts and F is the vector of applied loads at the end effector. When the robot is modeled with lumped compliance in the joints,

$$\tau = K\delta\theta \qquad (22)$$

K is a diagonal matrix where the eigenvalues represent the four local joint stiffnesses that can be controlled on each joint by the use of two agonist/antagonist actuators. K is alternately expressed as the inverse of the compliance matrix C, and therefore

$$\delta P = (JK^{-1}J^T)F = C_g F \qquad (23)$$

Here we use C_g to denote the global compliance matrix.

In the rehabilitation setting, this mapping of stiffness/compliance can be used to create assistance or resistance along an intended task path (stiffen the manipulator along the tangent direction), or to provide correction when deviation from the intended task path is encountered (stiffen the

manipulator normal to the tangent direction). These can be thought of as three main control modes (assistive, resistive, and corrective [14]) for robot-assisted rehabilitation. A passive mode (zero stiffness) may also be useful. In this analysis we neglect the considerations of friction and backdriveability attributable to the differentials, since the basic differential is highly efficient in comparison to gear reduction that would typically be found at the drive motors.

6 System Analysis

A precise model of the system is highly coupled and does not lend itself to a closed-form solution; the orientation of the force on the idler depends on the idler position and the resulting belt angles, but the orientation of the force influences the beam deflection and therefore the idler position itself. Therefore, a model is pursued which approximates beam deflection behavior based on a widely accepted model for large displacements of compliant beams, and assuming that stiffness of the belt is much greater than that of the compliant beam (i.e., the belt acts as a kinematic constraint (inextensible), with no pretension at the neutral position of the idler). As we can assume equal angles of the input and output wheels (neutral, or no relative displacement), the path of the idler (point P in Figure 4) allowed by the belt is an arc of an ellipse. The considered ellipse is described by its major and minor axis lengths, respectively a_e and b_e, as shown in Figure 5.

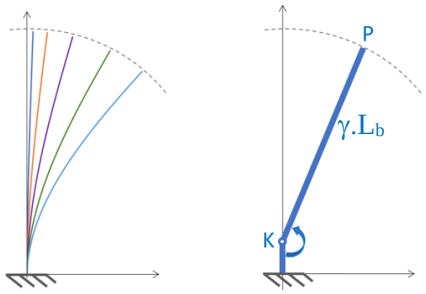

Fig. 4. Large-deflection beam model (left) and pseudo-rigid body model (right). The large displacement of the beam's extremity, in the beam support frame, is a circle centered at K.

.

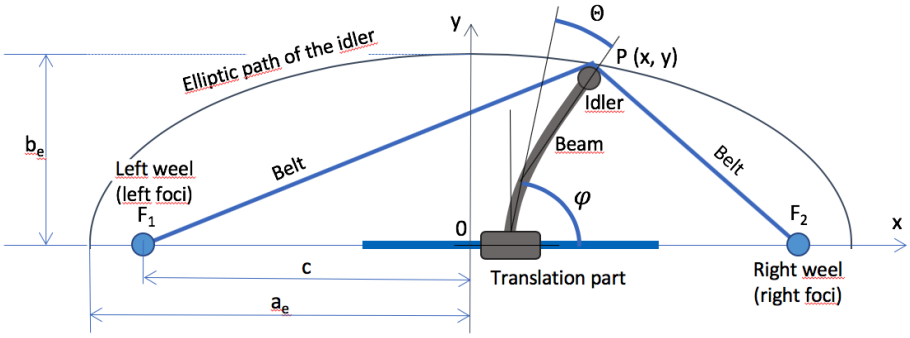

Fig. 5. Elliptical model of idler position (top and bottom left); beam model (bottom right).

With the focal distance c prescribed (the half-spacing of the input and output pulleys), and the minor axis set equal to the y-component of the undeflected beam (i.e., no preload in the beam as the idler travels across the top-most point of the ellipse), the ellipse axes are given by

$$b_e = L_b.\sin(\varphi) \qquad (24)$$

$$a_e = (c^2 + b_e^2)^{1/2} \quad (25)$$

According to the widely adopted pseudo-rigid body model of a compliant fixed-pinned beam of length L_b under tip loading with large deflections (nonlinear beam) [29], it has been shown that the beam tip traces an approximately circular deflection path, with the center of that path located a distance $L_b(1 - \gamma)$ from the base of the beam, and an equivalent torsion spring K located at the circle's center (see Figures 4 and 6). In other words, the equivalent rigid-body beam has length γL_b ($\gamma = 0.85$ gives a relatively accurate approximation for a range of loading orientations [29]). The undeflected beam is initially oriented at an angle φ, and the tip of the deflected beam under tip loading is at an angle of $(\varphi + \Theta)$, as in Figure 6.

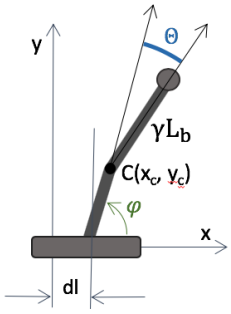

Fig. 6. Flexible beam model with displacements.

If the beam has an initial undeflected orientation φ (see Figure 6), and the beam/idler carriage is displaced a distance dl along the x-axis (see Figures 5 and 6), then the center of rotation of the equivalent beam is given by:

$$x_c = dl + L_b(1 - \gamma).\cos(\varphi) \quad (26)$$

$$y_c = L_b(1 - \gamma).\sin(\varphi) \quad (27)$$

The idler location P (x,y) is then found as the intersection of the circle with the ellipse by solving the set of equations

$$(x - x_c)^2 + (y - y_c)^2 = (\gamma L_b)^2 \quad (28)$$

$$(x/a_e)^2 + (y/b_e)^2 = 1 \quad (29)$$

This allows approximation of the (negative-valued) beam deflection angle Θ using

$$x = x_c + \gamma L_b.\cos(\varphi + \Theta) \quad (30)$$

$$y = y_c + \gamma L_b.\sin(\varphi + \Theta) \quad (31)$$

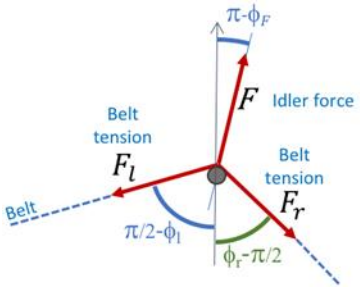

Fig. 7. Decomposition of belt forces and resultant in a pseudo-equilibrium of the idler (left and right belt tension magnitudes are equal.

The orientation of the force applied by the belt on the idler ϕ_F is then easily found by averaging the angles of the two (left and right) belt segments (i.e., the force bisects the angle made by the belt segments as shown in Figure 7):

$$\phi_l = \tan^{-1}(y/(x + c)) \quad (32)$$

$$\phi_r = \tan^{-1}(y/(x - c)) \quad (33)$$

$$\phi_F = (\phi_l + \phi_r)/2 + \pi \quad (34)$$

To solve for the compliant beam behavior, it is now necessary to improve on the initial approximation for γ, as beam stiffness is nonlinear in γ [29]. This value is sensitive to compressive loading along the beam, so it is helpful to define n as the ratio of longitudinal to transverse loading at the beam tip:

$$n = \cot(\phi_F - \varphi - \pi) \quad (35)$$

At this point, equations from [29] are used to refine γ and calculate K as functions of n. More specifically, a dimensionless stiffness factor K_Θ is a function of n (the reader is referred to [29] for further details), and

$$K = \gamma K_\Theta EI/L_b \quad (36)$$

where EI is the flexural stiffness of the beam. The moment at the base of the beam is then

$$M = K\Theta \quad (37)$$

and the transmission ratio relating the orientation of the force on the idler and the force generating transverse loading on the beam tip (i.e., the relative angle between the applied load and the beam tip orientation) is

$$\alpha = \sin(\phi_F - \Theta - \varphi) \quad (38)$$

The apparent stiffness K_{app} of the system is then proportional to

$$K_{app} \sim M/\alpha \quad (39)$$

which is adjustable through the carriage displacement dl. In other words, if the force applied from the belt through the idler onto the beam is normal to the deflected beam, the apparent stiffness is simply the stiffness of the beam, but if the force is along the beam length then the system appears "infinitely" stiff (up to the stiffness of the belt and other loaded components). It should be noted that since load applied at the joint will tend to deflect the beam and cause relative rotation between the input and output rotation axes (further stiffening the system), K_{app} should be thought of as a local approximation valid for small values of relative rotation. The additional nonlinear effect of stiffening through relative joint displacement is not explicitly considered in this model, based on the assumption that these deflections would be mitigated (or limited) through the use of an appropriate controller.

7 Example of Variable Stiffness Mechanism

The above analysis procedure was implemented in MATLAB software with nominal values of $c = 10$, $L_b = 4$, and $EI = 3$. Rather than focusing on these arbitrarily selected values, the objective is to investigate how the stiffness behavior changes with adjustments in θ and L_b. Notably, from the above equations, these two variables influence the aspect ratio of the ellipse as well as the effective transmission ratio. Values of L_b in the range [1 5] and values of φ in the range [0 π/2] were simulated. Here two sample results are given.

In Figure 8, the results for $L_b = 2$ and $\varphi = \pi/4$ are shown. One can observe that over a range of dl = [-2 7], the apparent stiffness changes by >10x, without excessive beam deflection (beam angle ratio < 1) and with horizontal load carried in the lead screw not exceeding about 35% of the tip load on the beam. In Figure 9, the results for $L_b = 4$ and $\varphi = \pi/6$ are shown. Noting the difference in stiffness scale between Figures 8 and 9, one can observe that over a range of dl = [-5 5], the apparent stiffness changes by about 20x, without excessive beam deflection (beam angle ratio < 1) and with horizontal load carried in the lead screw not exceeding about 40% of the tip load on the beam. This appears to be a slightly superior solution.

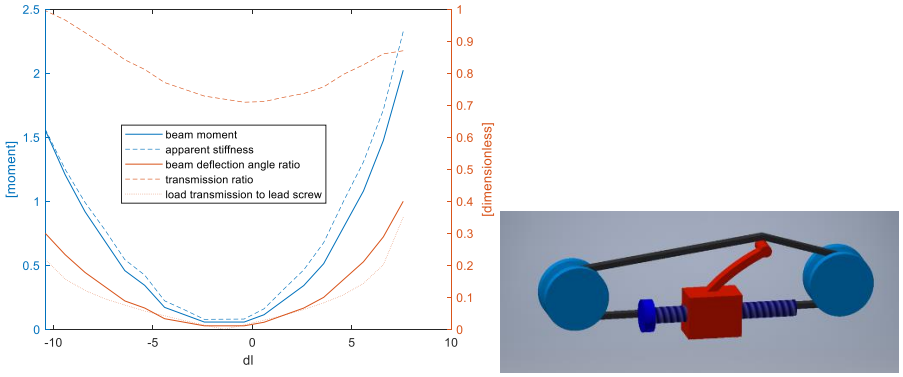

Fig. 8. Results for $L_b = 2$ and $\varphi = \pi/4$.

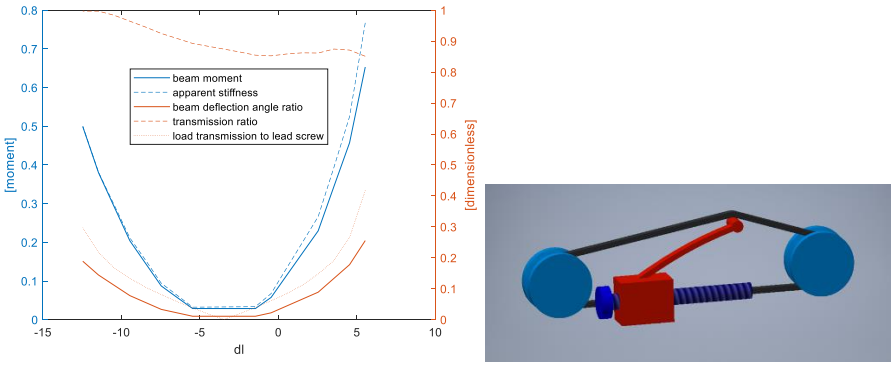

Fig. 9. Results for $L_b = 4$ and $\varphi = \pi/6$.

8 Examples of Robot Stiffness Behavior

We take as a first example a rectilinear motion to be traced by the human hand as a rehabilitation exercise, guided by the variable-stiffness robot. The task description is shown in Figure 10. Using reflective markers (placed on the shoulder, upper arm, elbow, forearm, wrist, and hand) and a

Vicon infrared camera system, typical human arm kinematics for this rectilinear motion was measured at 100 Hz as a benchmark. Such a movement is the expression of a prioritized, important objective for a patient: translation within a gravity field (functionally representing tasks such as reaching for and grasping an object) is a standard motif in rehabilitation.

The eigenvectors of the global compliance matrix represent directions along which an applied force will produce an aligned deflection. To avoid pushing the user off the intended trajectory, while controlling stiffness of the manipulator tangent to the path, the eigenvalues of the stiffness matrix should be tuned to align with the path tangent. This is done through optimization of the joint stiffnesses. At the same time, it is important to ensure that the robot and human only interact at the end effector, i.e., that the elbow or arm segments of the robot do not physically interfere with the elbow or arm segments of the human; this is the motivation for recording the benchmark of human motion as in Figure 10.

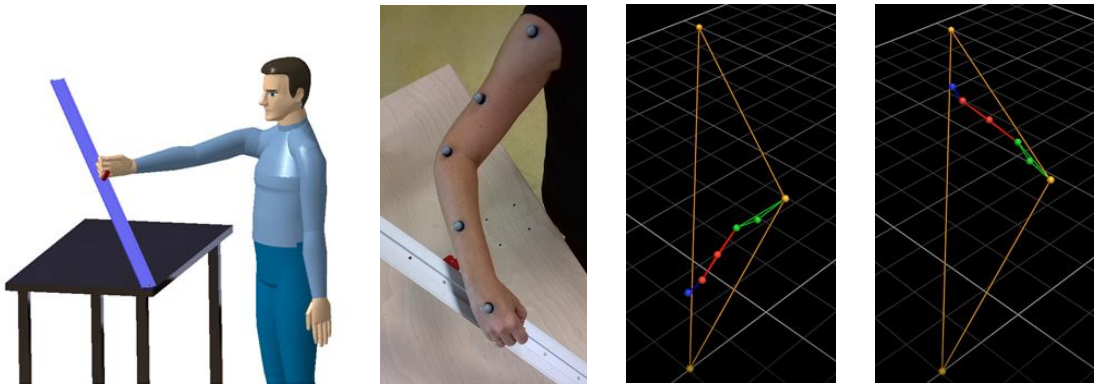

Fig. 10. Human arm motion task.

Experiments were conducted with individuals asked to follow the rectilinear hand trajectory shown in Figure 10. The results indicated globally very similar behavior.

In following the linear trajectory, person A demonstrates a behavior similar to what would be expected in pseudoinverse-based robot control (Figure 11 left). The elbow trajectory of person B also follows the equivalent pseudoinverse path, but with deviation that grows little by little along the path. In this second case (Figure 11 right), the resolution of redundancy was accomplished using an orthogonal projection (not detailed in this paper) to model the human behavior in the context of this arm movement.

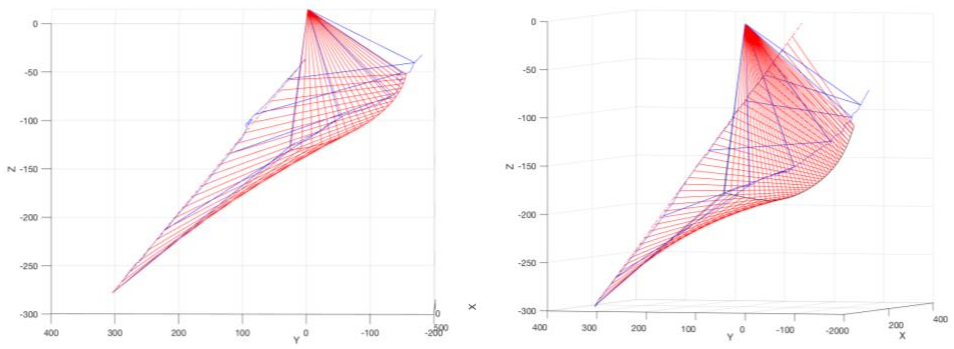

Fig. 11. Human arm motion (blue) and equivalent robot motion (red). Person A left; person B right.

The inverse kinematics approach described above was used to solve for the joint angles θ_i (and input angles ϕ_i) which produce the given trajectory with equal link lengths L_1 and L_2, subject to the constraint that the elbow of the robot should remain in the plane z = 0, as shown in Figure 12.

Using the Jacobian pseudoinverse solution approach, the joint trajectories are slightly different, as shown in Figure 13, and the efficiency of motion is apparent – the arm stays nearly in the plane of its initial pose, and although motion in θ_2 is now nonzero, variations in θ_1 and θ_4 are very slight, suggesting overall lower kinetic energy.

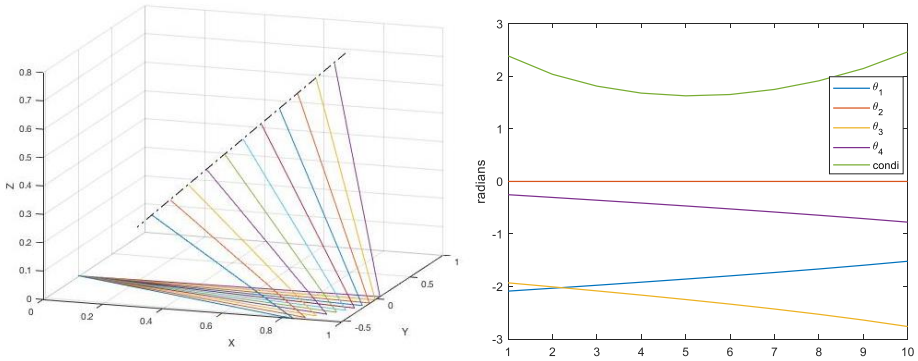

Fig. 12. Illustration of eleven successive kinematic solutions in the tracking of a straight-line trajectory (left) from $[0.2, 0.2, 0.2]^T$ to $[0.7, 0.7, 0.7]^T$ with the robot's elbow constrained to lie in the horizontal plane (z = 0). The four resulting joint angles (in radians) and condition number of the Jacobian matrix (right).

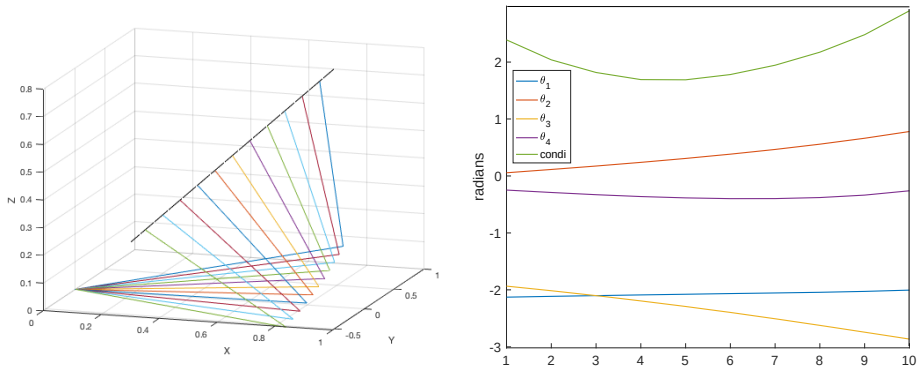

Fig. 13. Tracking a straight-line trajectory using the Jacobian pseudoinverse approach (left). The motion efficiency in the joint space is clear, but the elbow position cannot be specified as it depends on the previous robot configuration. Joint values and condition number of the Jacobian matrix (right).

For equally spaced positions along the trajectory with $P_{1z} = 0$, the input compliance values $c_{1\text{-}4}$ (the inverse of the input stiffness values) were treated as optimization variables in the range [0.01 10] using fmincon() in MATLAB, minimizing the angle between the desired trajectory direction vector and either of the two "strongest" eigenvectors (those with larger eigenvalues) of the global compliance matrix. The resulting compliance values (entries on the diagonal of C), and the angular misalignment of the compliance ellipsoid with the trajectory tangent, are shown in Figure 14.

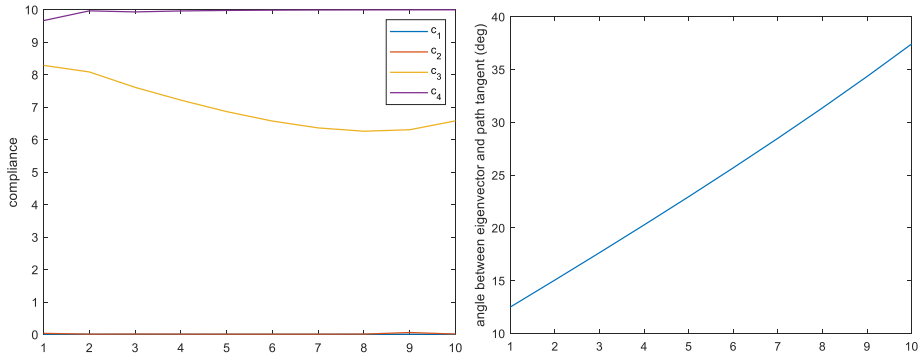

Fig. 14. Compliance values; angular misalignment of compliance ellipsoid (in the simulation of the constrained elbow pose).

It can be noticed that the optimizer pushes some of the component compliances (stiffnesses) to their upper and lower bounds. The severe angular misalignment evident in this example illustrates the difficulty of using positive-valued, bounded joint stiffness elements to orient the compliance ellipsoid when the position solution is fully constrained (i.e., without taking advantage of the robot's redundancy).

If, instead, the goal is to maintain relatively uniform compliance in all directions, the objective function is re-expressed in terms of the relative magnitude of the eigenvalues of the compliance matrix, i.e., maximizing the ratio of the minimum to maximum eigenvalue. This forces the compliance ellipsoid to be as spherical as possible. With this revised objective function, the variation of stiffness values is more within practical bounds (Figure 15), but the achievement of the goal is still somewhat elusive, with the aspect ratio of the compliance ellipsoid reaching above 4.5:1 for the given trajectory.

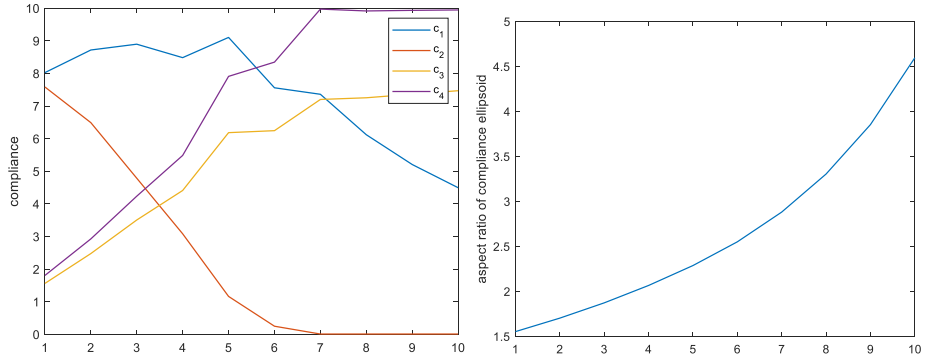

Fig. 15. Compliance values; aspect ratio of compliance (maximum to minimum eigenvalues).

Both robot motions with constrained z-plane (as in Figure 12) and with pseudoinverse control (as in Figure 13) are compared to the human reference motion in Figure 16. It can be seen that in both cases collisions between the robot elbow and arm segments with the human arm are avoided.

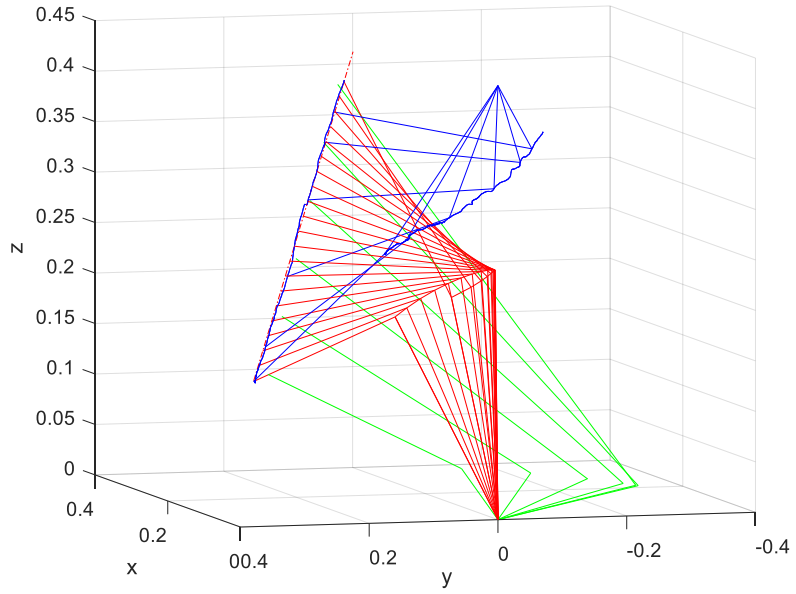

Fig. 16. Comparison of robot and human arm trajectories to check for interference; human in blue with shoulder location near top of figure; robot base at (0,0,0) with green indicating trajectory with z=0 constraint and red indicating pseudoinverse-based trajectory.

As a second example, also characteristic of a classic patient objective, we now take a helical trajectory as shown in Figure 17. The solution is calculated using the pseudoinverse method for the sequence of waypoints along the path. Once again we take as the goal to maintain relatively uniform compliance in all directions, i.e., maximizing the ratio of the minimum to maximum eigenvalue of the compliance matrix. The resulting compliance values and performance of the goal function are shown in Figure 18. One can notice that the compliance values stay nicely within bounds and the aspect ratio of the compliance ellipsoid is better than with the straight-line trajectory, though still not perfect.

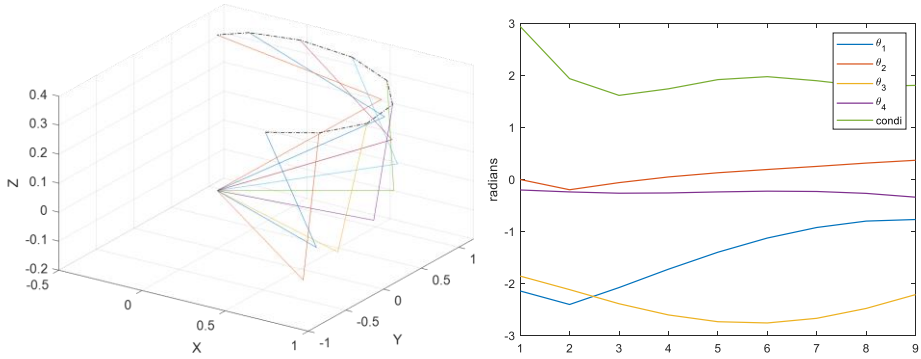

Fig. 17. Helical trajectory; joint angle solution and condition number of the Jacobian.

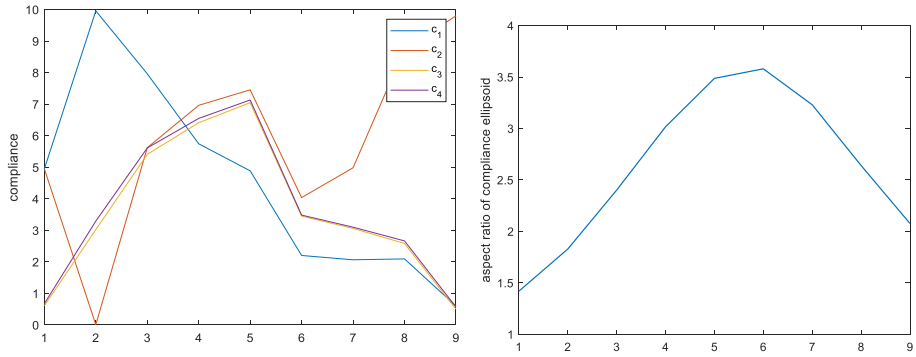

Fig. 18. Compliance values for helical trajectory; aspect ratio of compliance (maximum to minimum eigenvalues).

These results collectively suggest that the ability to robustly achieve objectives related to the compliance ellipsoid properties, and even compliance values in general, may be to take advantage of the robot redundancy. In other words, rather than constrain the kinematic solution (elbow location), the additional freedom of robot elbow placement may be used to improve the compliance optimization by changing the Jacobian and thereby changing the global compliance matrix. This bears further investigation.

9 Conclusions

In this paper, a mechanism providing variable stiffness for robotic rehabilitation and other human-interaction applications has been presented. By using a compliant beam and optimizing its length and orientation, a wide range of stiffness properties was achieved without requiring high performance of the stiffness adjustment actuator or introducing excessive complexity in the mechanism. This is expected to enable improved integration of "mechanical intelligence" in human-robot applications.

A redundant robot for upper limb rehabilitation with variable stiffness has also been presented. Its forward kinematics were given, and the robot's redundancy was used to obtain a simple inverse kinematic solution in closed form. Kinematic solutions with this method were compared with those from a Jacobian pseudoinverse approach. The effects of inserting variable-stiffness elements between the actuators and joint axes were described in terms of a mapping from local stiffness to global stiffness characteristics as embodied in the global compliance matrix. Experimental results showed that the eigen-properties of this matrix can be difficult to optimize in relation to meaningful rehabilitation tasks, without resorting to exploitation of the kinematic redundancy in order to explore a larger search space in the overall optimization; this latter approach merits further study in future work.

10 Acknowledgements

The work described in this paper was supported in part by the University of Orléans.

References

1. US Census Bureau. “The Nation's Older Population Is Still Growing,” Release CB17-100 (2017).
2. National Spinal Cord Injury Statistical Center. “Facts and Figures at a Glance,” Birmingham, AL: University of Alabama at Birmingham (2017).
3. Vanderborght, B., Albu-Schaeffer, A., Bicchi, A., Burdet, E., Caldwell, D.G., Carloni, R., Catalano, M., Eiberger, O., Friedl, W., Ganesh, G., Garabini, M., Grebenstein, M., Grioli, G., Haddadin, S., Hoppner, H., Jafari, A., Laffranchi, M., Lefeber, D., Petit, F., Stramigioli, S., Tsagarakis, N., Van Damme, M., Van Ham, R., Visser, L.C., Wolf, S. “Variable impedance actuators: A review,” Robotics and Autonomous Systems 61(12), 1601-1614, http://dx.doi.org/10.1016/j.robot.2013.06.009 (2013).
4. Reinkensmeyer, D.J., Kahn, L.E., Averbuch, M., McKenna-Cole, A., Schmit, B.D., Rymer, W.Z. “Understanding and treating arm movement impairment after chronic brain injury: progress with the ARM guide,” J Rehabil Res Dev 37, 653-662 (2000).
5. Staubli, P., Nef, T., Klamroth-Marganska, V., Riener, R. “Effects of intensive arm training with the rehabilitation robot ARMin II in chronic stroke patients: four single-cases,” J Neuroeng Rehabil 6, 46 (2009).
6. Hesse, S., Schulte-Tigges G., Konrad, M., Bardeleben, A., Werner, C. “Robot-assisted arm trainer for the passive and active practice of bilateral forearm and wrist movements in hemiparetic subjects,” Archives of Physical Medicine and Rehabilitation 84, 915-920 (2003).
7. Louriero, R., Amirabdollahian, F., Topping, M., Driesse, B., Harwin, W. “Upper limb robot mediated stroke therapy - GENTLE/s approach,” Auton Robots 15, 35-51 (2003).
8. Lum, P.S., Burgar, C.G., Shor, P.C., Majmundar, M., Van der Loos, M. “Robot-assisted movement training compared with conventional therapy techniques for the rehabilitation of upper-limb motor function after stroke,” Arch Phys Med Rehabil 83, 952-959 (2002).
9. Krebs, H.I., Hogan, N., Aisen, M.L., Volpe, B.T. “Robot-aided neurorehabilitation,” IEEE Trans Rehab Eng 1, 75-87 (1998).
10. Sanchez, R.J., Liu, J., Rao, S., Shah, P. Smith, R., Rahman, T., Cramer, S.C., Bobrow, J.E., Reinkensmeyer, D.J. “Automating arm movement training following severe stroke: functional exercises with quantitative feedback in a gravity-reduced environment,” IEEE Trans Neural Sys Rehab Eng 14, 378-389 (2006).
11. Housman, S.J., Scott, K.M., Reinkensmeyer, D.J. “A randomized controlled trial of gravity-supported, computer-enhanced arm exercise for individuals with severe hemiparesis,” Neurorehabilitation and Neural Repair 23, 505-514 (2009).
12. Zariffa, J., Kapadia, N., Kramer, J.L.K., Taylor, P., Alizadeh-Meghrazi, M., Zivanovic, V., Willms, R. Townson, A., Curt, A., Popovic, M.R., Steeves, D. “Feasibility and efficacy of upper limb robotic rehabilitation in a subacute cervical spinal cord injury population,” Spinal Cord 50, 220-226 (2012).

13. Maciejasz, P., Eschweiler, J., Gerlach-Hahn, K., Jansen-Troy, A., Leonhardt, S. "A survey on robotic devices for upper limb rehabilitation," Journal of NeuroEngineering and Rehabilitation 11, 3 (2014).
14. Proietti, T., Crocher, V., Roby-Brami, A., Jarrasse, N. (2016) Upper-limb robotic exoskeletons for neurorehabilitation: a review on control strategies. IEEE Rev Biomed Eng. DOI: 10.1109/RBME.2016.2552201.
15. Sugar, T. (2002) A novel selective compliant actuator. Mechatronics 12(9): 1157-1171.
16. Tsagarakis, N., Laffranchi, M., Vanderborght, B., Caldwell, D. (2009) A Compact Soft Actuator Unit for Small Scale Human Friendly Robots, in: IEEE International Conference on Robotics and Automation (ICRA 2009) pp. 4356-4362.
17. Palli, G., Berselli, G., Melchiorri, C., Vassura, G. (2011) Design of a Variable Stiffness Actuator Based on Flexures. ASME Journal of Mechanisms and Robotics 3: 034501 (5 pp.)
18. English, C., Russell, D. (1999) Implementation of variable joint stiffness through antagonistic actuation using rolamite springs, Mechanism and Machine Theory 34(1): 27–40.
19. Boehler, Q. (2016) Analyse, conception et commande de mécanismes de tenségrité et systèmes précontraints, PhD thesis, Univ. de Strasbourg.
20. Zhou, X., Jun, S.-K., Krovi, V. (2015) A Cable Based Active Variable Stiffness Module With Decoupled Tension. ASME Journal of Mechanisms and Robotics 7: 011005 (5 pp.).
21. Enoch. A., Vijayakumar, S. (2016) Rapid manufacture of novel variable impedance robots, ASME Journal of Mechanisms and Robotics 8: 011003 (11 pp.).
22. Hollander, K., T. (2004) Sugar, Concepts for compliant actuation in wearable robotic systems, in: US-Korea Conference on Science, Technology and Entrepreneurship (UKC2004).
23. Kawamura, S., Yamamoto, T., Ishida, D., Ogata, T., Nakayama, Y., Tabata, O., Sugiyama, S. (2002) Development of passive elements with variable mechanical impedance for wearable robots, in: IEEE International Conference on Robotics and Automation (ICRA 2002) 1: 248-253.
24. Kani, M. H. H., Bonabi, H. A. Y., Bidgoly, H. J., Yazdanpanah, M. J., Ahmadabadi, M. N. (2016) Design and Implementation of a Distributed Variable Impedance Actuator Using Parallel Linear Springs, ASME Journal of Mechanisms and Robotics, 8: 021024 (12 pp.).
25. Tsagarakis, N.I. Sardellitti, C.D.G. (2011) A new variable stiffness actuator (CompAct-VSA): Design and Modelling, 2011 IEEE/RSJ International Conference on Intelligent Robots and Systems, September 25-30, 2011, San Francisco, CA, USA, pp. 378 – 383.
26. Jafari, A., Tsagarakis, N., Caldwell, D.G. (2011) AwAS-II: A new actuator with adjustable stiffness based on the novel principle of adaptable pivot point and variable lever ratio, in: IEEE International Conference on Robotics and Automation (ICRA): 4638–4643.
27. Groothuis, S. S., Rusticelli, G., Zucchelli, A., Stramigioli, S., Carloni, R. (2012) The vsaUT-II: a novel rotational variable stiffness actuator, in: IEEE International Conference on Robotics and Automation (ICRA 2012).
28. Fumagalli, M., Barrett, E., Stramigioli, S., Carloni, R. (2012) The mVSA-UT: a miniaturized differential mechanism for a continuous rotational variable stiffness actuator, in: 4th IEEE RAS

& EMBS International Conference on Biomedical Robotics and Biomechatronics (BioRob 2012): 1943-1948.

29. Howell, L. L. (2001) *Compliant Mechanisms*, John Wiley & Sons.